Evolution of Vesicle Release Mechanisms in Neuro-Spike Communication

Yu Wenlong and Lin Lin(✉)

College of Electronics and Information Engineering, Tongji University, Shanghai 201804, China
fxlinlin@tongji.edu.cn

Abstract. Neuro-spike communication has become a hot topic and has been investigated extensively in recent years. The vesicle release process is the main part of neuro-spike communication, which directly determines the accuracy of information transmission. Currently, single vesicle release (SVR) model is used to investigate the process of vesicle release, but there is few research on multi-vesicle release (MVR) model. In this paper, a pool-based MVR model is presented, and the influence of data rate and several system parameters on bit error rate (BER) performance of the model is simulated. In addition, the BER performance of SVR model and MVR model under the same conditions is compared. The advantages and disadvantages of the two models are analyzed.

Keywords: Molecular communication · Neuro-spike communication · Nanonetworks · Vesicle release process · Bit error rate

1 Introduction

As the most promising candidate for reliable communications at nano- or micro-scale, molecular communication has attracted much attention in recent years. Great progress has been made in the research on molecular communication. Many kinds of molecular communication systems have been investigated such as molecular communication via diffusion [11–13,15,25,32], microtubule-based communication [4,24], pheromone signaling [8], and bacteria-based communication [9].

Neuro-spike communication is a kind of communication method that includes electrical process and molecular communication process. The performance of

This work is supported in part by National Natural Science Foundation, China (61971314), in part by Science and Technology Commission of Shanghai Municipality (19510744900), and in part by Sino-German Center of Intelligent Systems, Tongji University.

T. Nakano (Ed.): BICT 2021, LNICST 403, pp. 105–116, 2021.
https://doi.org/10.1007/978-3-030-92163-7_9

neuro-spike communications is quite good in terms of reliability, speed and robustness [5]. The analysis of this communication paradigm is beneficial to exploit in the artificial neural systems where nanomachines are linked to neurons to treat the neurodegenerative diseases [23]. Therefore, research on neuro-spike communication has become a hot pot.

Many works have been done in the neuro-spike communication field. Several communication channel models have been introduced for every biological processes of this communication system [2,26,31]. To characterize the fundamental properties of neuro-spike communication, a physical channel model was proposed in [2]. Reference [20] proposed a synaptic model which shows that redundancy of synapses increases the information transmission efficiency. An alternative representation of the neuron-to-neuron communication method was proposed in [31] where the biological processes are modeled by their frequency responses. The vital events during the synaptic transmission were investigated in [21]. As the major part of neuro-spike communication, vesicle release process has received much attention.

Vesicle release is the process that the spike propagating to the end of the axon prompts the pre-synaptic terminals to release vesicles into gaps. Many vesicle release models have been investigated. In [31], a model which has the fixed vesicle release probability is utilized. There were finite state markov channels model used in [2] and pool-based release model used in [19,22]. However, the pool-based model is not realistic, where the number of available vesicles are overestimated since the refill rate is assumed to be proportional to the number of reserve vesicles. A realistic pool-based model for vesicle release and replenishment was proposed in [27], in which channel characteristics of neuro-spike communication systems have been investigated. These models only study the single vesicle release (SVR) process, and there is limited research on multi-vesicle release (MVR) models. But in fact, the SVR was originally thought to liberate at most one vesicle for each spike, rendering synaptic transmission unreliable. MVR, which was initially identified at specialized synapses but is now known to be common throughout the brain [28], represents a simple mechanism to overcome the intrinsic unreliability of synaptic transmission.

This paper presents a pool-based MVR and replenishment model. The BER performance of this model is investigated under different conditions comparing with that of SVR model. The release process of the two model have been introduced in [22]. Only a vesicle is released in response to a spike that inhibits the release of other vesicles in SVR process, while the number of vesicles released is random when a spike arrives in MVR process. The vesicle replenishment process is described in [27]. Besides, the influence of parameters of the two vesicle release models and data transmission rate on error probability is simulated. We compare the BER performance of the two models under different conditions and analyze the reasons in detail. The main contributions of this paper lie in several aspects:

– A realistic MVR model is presented to investigate the BER performance.
– The influence of parameters involved in the vesicle release process and data rate on BER performance is investigated in detail.

The remainder of this paper is organized as follows. Section 2 introduces the system model of neuro-spike communication. In Sect. 3, the vesicle release process of two vesicle release models is analyzed. The BER of two models is simulated under different conditions by MATLAB in Sect. 4. The influence of different parameters on BER is investigated and the reasons are analyzed. Finally, Sect. 5 concludes this paper.

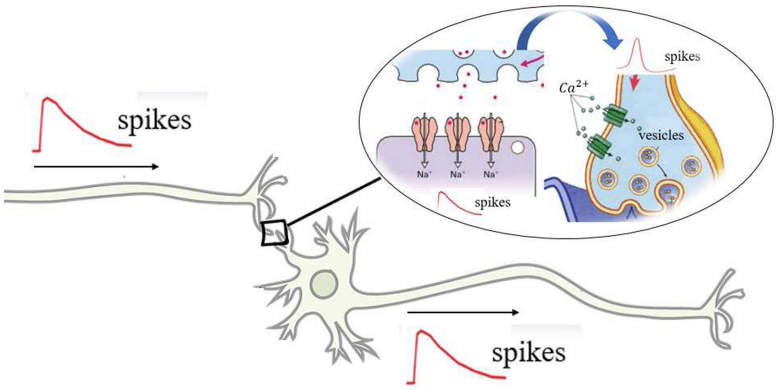

Fig. 1. The neuro-spike communication process. When a spike arrives at the end of the axon, the pre-synaptic terminals will release vesicles into gaps. The neurotransmitters released by the vesicles arrive at postsynaptic receptor after diffusion, and a new spike is formed on the next neuron.

2 System Model

The human nervous system contains billions of interconnected neurons that communicate with each other through synapses. The neuron is in a resting manner and is polarized with an intracellular potential about −95 to −65 mV when no signal is transmitted via the nervous system [10]. The nervous system transmits signals by electrically charged ion flows of potassium (K^+), sodium (Na^+), chloride (Cl^-). To transmit signals, neuron membrane potential can be changed by ion exchange between inside and outside of the neuron, which enter the neuron or exit from that via the ion channels located on the soma and dendrites (cation and anion channels) and on the nodes of Ranvier (Sodium and potassium channels). The potential increases high enough about 20 mV, the neuron will be excited and the membrane will be depolarized. Then, the firing will happen. When a neuron fires, an spike about 90 mV at a time period of 1 ms will be generated in the neuron. When a spike reaches an axon terminal, the depolarization leads to opening the calcium channels and causes an influx of calcium ions

(Ca^{2+}) into the pre-synaptic neuron [16], which leads to the release of neurotransmitters into the synapse gap. Neurotransmitters bind to the receptor of the postsynaptic neuron and make the cation or anion channel open by changing of permeability features of the neuron as shown in Fig. 1. Opening cation channels conduct positively charged ions into the neuron, and thus, increases its potential and leads to a spike firing.

Neuro-spike communication model is a hybrid model that involves both molecular communication in synaptic transmission part, and electrical transmission of action potentials in the axonal pathway. The traditional neuro-spike communication model is generally divided into three phases based on the biological process [1].

The first phase is the axonal transmission, that the spikes are propagated along the axon. When a spike arrives, the input symbol is considered to be "1". If no spike arrives, the input symbol is considered to be "0". Hence, the input $s(t)$ of pre-synaptic neuron can be viewed as a series of impulse signals:

$$s(t) = \sum_i \delta(t - t_i), \tag{1}$$

where $\delta(\cdot)$ is the delta function.

When the spike propagates to the end of the axon and changes the membrane potential of the neuron, the influx of calcium ions causes the pre-synaptic terminals to release vesicles containing neurotransmitters into gaps among neurons, which is the second phase. The pool-based vesicle release model is considered, which is shown in Fig. 2.

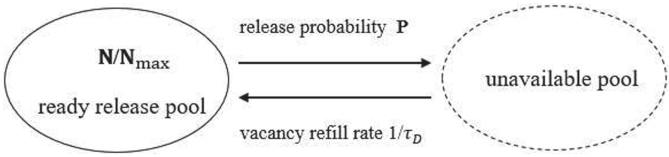

Fig. 2. Pool-based vesicle release model.

Readily releasable vesicles (RRVs) are stored in a pool with an upper limit of $N_{\max}$ called ready pool (RP), while the others are contained in a larger unavailable pool away from the pre-synaptic. Once a vesicle is released, there is a vacancy in RP and the vesicles farther away from the pre-synaptic are refilled into RP until the number of vesicles reaches $N_{\max}$. It is assumed that the number of ready to be docked in neurons is much higher than $N_{\max}$ and the recovery of each vacancy is independent of others. So the recovery of a vacancy can be modeled by the first event from a Passion process [27]. Therefore, in a symbol interval, the probability of one vacancy replenishment P_{rep} is described as:

$$P_{rep} = 1 - \exp(-{\tau_D}^{-1} T_s), \tag{2}$$

where τ_D is the mean recovery time of a vacancy [22]. The number of vesicles recovered after Δt obeys the Binomial distribution $B(N_{\max} - N, P_{rep})$. The vesicle release process is described by the following two models.

In the SVR model introduced in [27], when input symbol is "1" and the number of RRVs in RP N is larger than 0, a RRV is released as a result. At the same time, it transiently prevents other vesicles from being released [14]. Based on [7], the probability that no RRVs is released per stimulus is $\exp(-a_v N)$ for RP with N RRVs ($0 < N \leq N_{\max}$), where a_v is the vesicle fusion rate. Therefore, the release probability of a RRV P_s when there are N RRVs in RP is depicted as

$$P_s = 1 - \exp(-a_v N). \tag{3}$$

Besides, the vesicle fusion rate a_v is related to the number of vesicles N in RP [7] and can be expressed as

$$a_v = k_a \sqrt{N}, \tag{4}$$

where k_a is a positive coefficient. Therefore, (3) can also be described as

$$P_s = 1 - \exp(-k_a N^{\frac{3}{2}}). \tag{5}$$

A pool-based MVR model is presented in this paper. In this model, MVR is allowed and individual vesicles are released independently of each other. Therefore, the release probability of a RRV P_m is expressed as

$$P_m = 1 - \exp(-a_v) = 1 - \exp(-k_a \sqrt{N}). \tag{6}$$

So when input symbol is "1" and the RP contains N RRVs, the number of vesicles released obeys the binomial distribution $B(N, P_m)$.

Assuming that the symbol interval T_s is larger than the pulse duration, $s(t)$ can be described as

$$s(t) = \sum_{i=1}^{K} N_i a_i \delta(t - (i-1)T_s), \tag{7}$$

where a_i is the ith input symbol, K is the length of input signal, N_i is the number of neurotransmitters in all vesicles released for the first symbol.

The final phase is that the neurotransmitter spreads to the postsynaptic receptor and binds to it, forming a new spike on the next neuron and completing the transmission of information between neurons. Based on Fick's second law of diffusion which states that at time t, at position x, the molecular concentration $C(x,t)$ can be described by

$$\frac{1}{D} \frac{\partial C(x,t)}{\partial t} = \nabla^2 C(x,t), \tag{8}$$

where D is the diffusion coefficient of the medium, ∇^2 is Laplacian operator. The channel model proposed in [17] is utilized. Particle re-uptake at the presynaptic neuron can be modeled as irreversible adsorption to the homogeneous left

boundary. The radiating boundary condition modeling pre-synaptic re-uptake is given as

$$D\frac{\partial C(x,t)}{\partial x} = k_r C(x,t), \text{at } x = 0, \tag{9}$$

where k_r is the re-uptake coefficient. For the right boundary, the radiating boundary needs to be extended to incorporate particle desorption. Particle desorption is modeled as a first-order process depending on the intrinsic desorption rate k_d and on the amount of currently adsorbed particles, as

$$D\frac{\partial C(x,t)}{\partial x} = -k_f C(x,t) - k_d \int_0^t D\frac{\partial C(x,\tau)}{\partial x} d\tau, \text{at } x = d, \tag{10}$$

where k_f is the effective association coefficient.

Based on (7), the number of neurotransmitters released at $t = 0$ can be modeled with the initial value as

$$C(x,0) = N_1 \delta(x). \tag{11}$$

By finding the $C(x,t)$ that satisfies (8), (9), (10) and (11), the channel impulse response $h(t)$ can be expressed as

$$h(t) = \int_0^t -D\frac{\partial C(x,\tau)}{\partial x}\bigg|_{x=d} d\tau, \tag{12}$$

where d is the length of synaptic gap. So the response of channel $y(t)$ after free diffusion is

$$y(t) = s(t) * h(t), \tag{13}$$

where symbol $*$ indicates the convolution operation.

The energy difference based detection method is used to receive the signal according to [18].

3 Theoretical Analysis

When an impulse arrives at the end of axon, the MVR model may release more vesicles than SVR model under the same conditions. But at the same time, the MVR model with more vacancies may also have a higher number of vesicle replenishment. Then, it is difficult to compare vesicle consumption rates between the two models. Therefore, the two release models are analyzed in detail in this section.

Assuming that there are N vesicles in RP at time t ($0 < N < N_{\max}$). The vesicles replenishment process of the two vesicle release models is the same according to Sect. 2. For SVR model, the number of vesicles in RP is N_s at $t+T_s$ ($N - 1 \leq N_s \leq N_{\max}$). The corresponding probability is:

$$\begin{aligned}
P_r(N_s = N-1) &= (1-P_{rep})^{N_{\max}-N} P_s, \\
P_r(N_s = N) &= (1-P_{rep})^{N_{\max}-N}(1-P_s) \\
&\quad + (1-P_{rep})^{N_{\max}-N-1} P_s, \\
&\cdots \\
P_r(N_s = N+i) &= \binom{i}{N_{\max}-N}(1-P_{rep})^{N_{\max}-N-i} P_{rep}^{i}(1-P_s) \\
&\quad + \binom{i+1}{N_{\max}-N}(1-P_{rep})^{N_{\max}-N-i-1} P_{rep}^{i-1} P_s, \\
&\cdots \\
P_r(N_s = N_{\max}) &= P_{rep}^{N_{\max}-N}(1-P_s).
\end{aligned} \tag{14}$$

For simplicity, P_i is used to express $P_r(N_s = N+i)$ $(-1 \le i \le N_{\max} - N)$. According to the knowledge of probability theory, vesicle release and recovery process are independent of each other. Hence the mean of the variation number of vesicles in RP is described as

$$E_s = \sum_{i=-1}^{N_{\max}-N} i \times P_i = E_{rep1} + E_{rel1}, \tag{15}$$

where E_{rep1} is the mean of vesicle recovery process and E_{rel1} is the mean of vesicle release process. Therefore,

$$E_s = (N_{\max} - N)P_{rep} - P_s. \tag{16}$$

In the same way, the mean of the variation number of vesicles in RP for MVR model is depicted as

$$E_m = (N_{\max} - N)P_{rep} - NP_m. \tag{17}$$

Based on (2)–(6), it can be seen that both E_s and E_m are functions of N. To investigate the properties of these two mean functions, the derivatives of E_s and E_m are obtained, as

$$\begin{aligned}
\frac{\mathrm{d}E_s(N)}{\mathrm{d}N} &= -P_{rep} - \frac{3k_a\sqrt{N}}{2}\exp(-k_a N^{3/2}), \\
\frac{\mathrm{d}E_m(N)}{\mathrm{d}N} &= -P_{rep} - 1 + \exp(-k_a N^{1/2}) - \frac{k_a\sqrt{N}}{2}\exp(-k_a N^{1/2}),
\end{aligned} \tag{18}$$

where P_{rep}, k_a and N are all larger than 0. From (18), it can be seen that both $\frac{\mathrm{d}E_s(N)}{\mathrm{d}N}$ and $\frac{\mathrm{d}E_m(N)}{\mathrm{d}N}$ are smaller than 0 when $N \in [0, N_{\max}]$. Hence $E_s(N)$ and $E_m(N)$ are both monotonically decreasing functions of N. In addition, based on (16) and (17), we obtain

$$\begin{aligned}
E_s(0) &= N_{\max}P_{rep} > 0, \\
E_s(N_{\max}) &= -1 + \exp(-k_a {N_{\max}}^{3/2}) < 0, \\
E_m(0) &= N_{\max}P_{rep} > 0, \\
E_m(N_{\max}) &= -N_{\max}(1 - \exp(-k_a {N_{\max}}^{1/2})) < 0.
\end{aligned} \tag{19}$$

So both $E_s(N)$ and $E_m(N)$ have unique zero point in $(0, N_{\max})$, which can be obtained by solving $E_s(N) = 0$ and $E_m(N) = 0$. x is used to represent $\sqrt{N}$ in (16) and (17) for simplicity, which is expressed as

$$\begin{aligned} f_s(x) &= (N_{\max} - x^2)P_{rep} - 1 + \exp(-k_a x^3) = 0, \\ f_m(x) &= (N_{\max} - x^2)P_{rep} - x^2(1 - \exp(-k_a x)) = 0, \end{aligned} \tag{20}$$

where $x \in (0, \sqrt{N_{\max}})$. After simplification, Eq. (20) can be expressed as

$$\begin{aligned} x_s^3 + \frac{1 - N_{\max}P_{rep}}{P_{rep}} x_s + \frac{2}{3k_a} &= 0, \\ x_m^3 - \frac{N_{\max}P_{rep}}{1 + P_{rep}} x_m + \frac{2}{k_a}\frac{N_{\max}P_{rep}}{1 + P_{rep}} &= 0, \end{aligned} \tag{21}$$

where x_s, x_m are the zero points of $f_s(x) = 0$ and $f_m(x) = 0$, respectively. Based on Cardano formula [30], we can obtain

$$\begin{aligned} x_s &= (-\frac{q_s}{2} + \sqrt{\frac{r_s^3}{27} + \frac{q_s^2}{4}})^{1/3} + (-\frac{q_s}{2} - \sqrt{\frac{r_s^3}{27} + \frac{q_s^2}{4}})^{1/3}, \\ x_m &= (-\frac{q_m}{2} + \sqrt{\frac{r_m^3}{27} + \frac{q_m^2}{4}})^{1/3} + (-\frac{q_m}{2} - \sqrt{\frac{r_m^3}{27} + \frac{q_m^2}{4}})^{1/3}, \end{aligned} \tag{22}$$

where,

$$\begin{aligned} q_s &= \frac{1 - N_{\max}P_{rep}}{P_{rep}}, \\ r_s &= \frac{2}{3k_a}, \\ q_m &= -\frac{N_{\max}P_{rep}}{1 + P_{rep}}, \\ r_m &= \frac{2}{k_a}\frac{N_{\max}P_{rep}}{1 + P_{rep}}. \end{aligned} \tag{23}$$

Besides, among x_s and x_m which are obtained by solving (22), only those satisfying $x_s, x_m \in (0, \sqrt{N_{\max}})$ are wanted.

Their physical meaning can be described: When the time is long enough, the number of vesicles in RP of SVR model will converge to N_{s0} which is equal to x_s^2. As long as $N < N_{s0}$, $E_s(N) > 0$ which means that the vesicle refill rate is larger than release rate. In the same way, the vesicle refill rate is lower than release rate as $N > N_{s0}$. N_{m0} equal to x_m^2 is the convergence value of the vesicle number in RP after a long enough period for MVR model.

4 Simulation Results

Considering the influence of the duration of a spike on vesicle release, the time is discretized into windows with equal width Δt. The window size is selected to

ensure that at most one spike exists in each time window. In the simulations of this paper, the width of time window is set equal to the spike duration. Based on [3], $\Delta t = \Delta t_s = 4\,\text{ms}$. Hence, the symbol interval T_s is described as

$$T_s = k_s \Delta t, \tag{24}$$

where k_s is a positive coefficient and set to be a integer. The data rate is defined as $1/T_s$.

What's more, the mean recovery time τ_D is related to the capacity of the RP [27], as

$$\tau_D = \frac{k_D}{N_{\max}}, \tag{25}$$

where k_D is also a positive coefficient. Default values for simulation parameters are given below: $T_s = 16\,\text{ms}$, bit length $K = 10^4$, $a_v = 0.06\sqrt{N}$ [7], $N_{\max} = 10$ [29], $\tau_D = \frac{600}{N_{\max}}$ ms [6].

The influence of mean recovery time τ_D on BER is simulated. In each simulation, τ_D changes from 20 to 100 ms with the step of 10 ms. BER for systems utilizing SVR and MVR models with different τ_D is shown in Fig. 3(a).

From Fig. 3(a), it can be seen that the BER of two system models increases as τ_D increases. When τ_D is large, the vesicle replenishment probability is low based on (2) and it will limit the vesicle replenishment rate. Therefore, there are fewer RRVs than the model with smaller τ_D. According to (5), the low number of RRVs will decrease the probability of vesicle release, which will increase the BER.

Then, the influence of capacity of RP $N_{\max}$ on BER is simulated. In each simulation, $N_{\max}$ changes from 5 to 45 with the step of 5. The relationships between BER of the two systems and $N_{\max}$ are simulated and depicted in Fig. 3(b).

Figure 3(b) indicates that larger $N_{\max}$ will cause lower BER of communication model. Even when $N_{\max}$ is large enough, the BER of both systems decreases to 0. When $N_{\max}$ is large, the average recovery time of a vacancy is shorter according to (25). Therefore, there are more vesicles in RP and the vesicle release probability is larger, which leads to a lower BER.

Subsequently, the influence of data rate on BER is simulated. In each simulation, Symbol interval changes from 4 to 36 ms with the step of 4 ms. The relationships between BER of different systems and data rate are simulated and depicted in Fig. 3(c).

Based on the relationship between symbol interval and data rate, when the symbol interval increases, data rate will decrease. As can be seen from Fig. 3(c), the BER gradually decreases with the decrease of data rate. The reason is, the consumption rate of RRVs will be higher when the data rate is high, resulting in smaller RRVs in RV. Hence, the BER will decrease with the decrease of data rate.

The influence of fusion rate a_v is simulated finally. k_a changes from 0.01 to 0.46 with the step of 0.05. The BER of the two models with different a_v is calculated and shown in the Fig. 3(d).

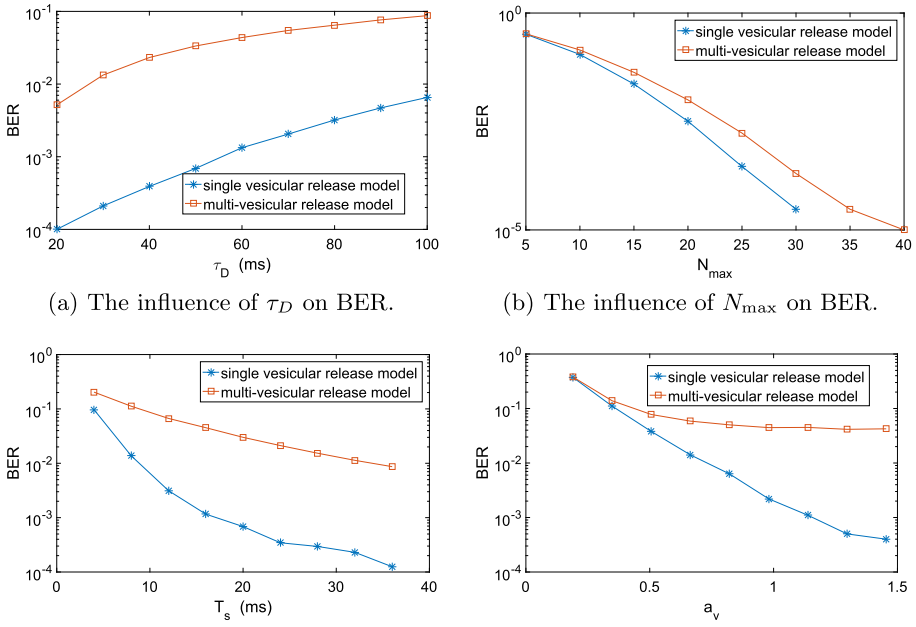

(a) The influence of τ_D on BER.

(b) The influence of $N_{\max}$ on BER.

(c) The influence of T_s on BER.

(d) The influence of a_v on BER.

Fig. 3. The influence of parameters on the BER performance of two vesicle release models.

In Fig. 3(d), the relationship between vesicle fusion rate a_v and BER is simulated and shown in Fig. 3(d). From (3) and (6), the increase of a_v will directly reduce the probability of vesicle release, resulting in more error detection cases.

In addition, it can be seen from the Fig. 3 that the BER of SVR model is always lower than the MVR model under the same conditions. This is because the vesicle depletion rate of the MVR model is much higher than that of the SVR model. Therefore, the number of vesicles in RP remains small and the possibility of vesicle depletion is much higher than that in the SVR model. This indicates that limiting the number of vesicles released will increase the transmission accuracy and make more effective use of limited resources to some extent. Also, the BER of SVR model is all more sensitive to the change of parameter than MVR model for Fig. 3. This is because the release of multiple vesicles greatly reduces the contingency of vesicle release and increases the stability of the model.

5 Conclusion

In this paper, a pool-based MVR model is proposed. The influence of data rate, mean vesicle recovery time, capacity of RP and vesicle fusion rate on BER performance of this model is simulated comparing with that of SVR model. From the simulation results, the BER of two models will increase as data rate and mean

recovery time of a vacancy increase, while it will decrease when the capacity of RP and vesicle fusion rate become larger. All the parameters change BER by influencing vesicle release probability. Compared with SVR model, MVR model has higher BER under the same conditions but has better stability. That is, all these parameters have greater influence on the BER performance of the SVR model.

References

1. Aghababaiyan, K., Maham, B.: Error probability analysis of neuro-spike communication channel. In: Proceedings of the IEEE Symposium on Computers and Communications (ISCC), pp. 932–937. IEEE (2017)
2. Balevi, E., Akan, O.B.: A physical channel model for nanoscale neuro-spike communications. IEEE Trans. Commun. **61**(3), 1178–1187 (2013)
3. Bear, M.F., Connors, B.W., Paradiso, M.A.: Neuroscience: Exploring the Brain (2007)
4. Darchini, K., Alfa, A.S.: Molecular communication via microtubules and physical contact in nanonetworks: a survey. Nano Commun. Netw. **4**(2), 73–85 (2013)
5. Dayan, P., Abbott, L.: Neuroscience: Computational and Mathematical Modeling of Neural Systems. MIT Press, Cambridge (2001)
6. De La Rocha, J., Parga, N.: Short-term synaptic depression causes a non-monotonic response to correlated stimuli. J. Neurosci. **25**(37), 8416–8431 (2005)
7. Dobrunz, L.E., Stevens, C.F.: Heterogeneity of release probability, facilitation, and depletion at central synapses. Neuron **18**(6), 995–1008 (1997)
8. Giné, L.P., Akyildiz, I.F.: Molecular communication options for long range nanonetworks. Comput. Netw. **53**(16), 2753–2766 (2009)
9. Gregori, M., Akyildiz, I.F.: A new nanonetwork architecture using flagellated bacteria and catalytic nanomotors. IEEE J. Sel. Areas Commun. **28**(4), 612–619 (2010)
10. Hosseini, M., Ghazizadeh, R., Farhadi, H.: A model for electro-chemical neural communication. In: Alam, M.M., Hämäläinen, M., Mucchi, L., Niazi, I.K., Le Moullec, Y. (eds.) BODYNETS 2020. LNICST, vol. 330, pp. 137–150. Springer, Cham (2020). https://doi.org/10.1007/978-3-030-64991-3_10
11. Huang, L., Lin, L., Liu, F., et al.: Clock synchronization for mobile molecular communication systems. IEEE Trans. Nanobiosci. **20**(4), 406–415 (2021)
12. Huang, S., Lin, L., Guo, W., et al.: Initial distance estimation and signal detection for diffusive mobile molecular communication. IEEE Trans. Nanobiosci. **19**(3), 422–433 (2020)
13. Huang, S., Lin, L., Xu, J., Guo, W., et al.: Molecular communication via subdiffusion with a spherical absorbing receiver. IEEE Wirel. Commun. Lett. **9**(10), 1682–1686 (2020)
14. Korn, H., Mallet, A., Triller, A., et al.: Transmission at a central inhibitory synapse. II. Quantal description of release, with a physical correlate for binomial n. J. Neurophysiol. **48**(3), 679–707 (1982)
15. Kuran, M.Ş, Yilmaz, H.B., Tugcu, T., et al.: Energy model for communication via diffusion in nanonetworks. Nano Commun. Netw. **1**(2), 86–95 (2010)
16. Lai, K.O., Ip, N.Y.: Central synapse and neuromuscular junction: same players, different roles. Trends Genet. **19**(7), 395–402 (2003)

17. Lotter, S., Ahmadzadeh, A., Schober, R.: Channel modeling for synaptic molecular communication with re-uptake and reversible receptor binding. In: Proceedings of the IEEE International Conference on Communications (ICC), pp. 1–7. IEEE (2020)
18. Luo, C., Wu, X., Lin, L., et al.: Non-coherent signal detection technique for mobile molecular communication at high data rates. In: Proceedings of the IEEE GLOBECOM, pp. 1–6. IEEE (2019)
19. Malak, D., Akan, O.B.: A communication theoretical analysis of synaptic multiple-access channel in hippocampal-cortical neurons. IEEE Trans. Commun. **61**(6), 2457–2467 (2013)
20. Manwani, A.: Information-theoretic analysis of neuronal communication. Ph.D. thesis, California Institute of Technology (2000)
21. Manwani, A., Koch, C.: Detecting and estimating signals over noisy and unreliable synapses: information-theoretic analysis. Neural Comput. **13**(1), 1–33 (2001)
22. Matveev, V., Wang, X.J.: Implications of all-or-none synaptic transmission and short-term depression beyond vesicle depletion: a computational study. J. Neurosci. **20**(4), 1575–1588 (2000)
23. Mesiti, F., Balasingham, I.: Nanomachine-to-neuron communication interfaces for neuronal stimulation at nanoscale. IEEE J. Sel. Areas Commun. **31**(12), 695–704 (2013)
24. Moore, M., Enomoto, A., Nakano, T., et al.: A design of a molecular communication system for nanomachines using molecular motors. In: Proceedings of the 4th Annual IEEE International Conference on Pervasive Computing and Communications Workshops (PERCOMW 2006), pp. 6–pp. IEEE (2006)
25. Nakano, T., Eckford, A.W., Haraguchi, T.: Molecular Communication. Cambridge University Press, Cambridge (2013)
26. Ramezani, H., Akan, O.B.: A communication theoretical modeling of axonal propagation in hippocampal pyramidal neurons. IEEE Trans. Nanobiosci. **16**(4), 248–256 (2017)
27. Ramezani, H., Akan, O.B.: Information capacity of vesicle release in neuro-spike communication. IEEE Commun. Lett. **22**(1), 41–44 (2017)
28. Rudolph, S., Tsai, M.C., von Gersdorff, H., et al.: The ubiquitous nature of multivesicular release. Trends Neurosci. **38**(7), 428–438 (2015)
29. Schikorski, T., Stevens, C.F.: Quantitative ultrastructural analysis of hippocampal excitatory synapses. J. Neurosci. **17**(15), 5858–5867 (1997)
30. Tokunaga, H.: Triple coverings of algebraic surfaces according to the Cardano formula. J. Math. Kyoto Univ. **31**(2), 359–375 (1991)
31. Veletić, M., Floor, P.A., Babić, Z., et al.: Peer-to-peer communication in neuronal nano-network. IEEE Trans. Commun. **64**(3), 1153–1166 (2016)
32. Zheng, R., Lin, L., Yan, H.: A noise suppression filter for molecular communication via diffusion. IEEE Wirel. Commun. Lett. **10**(3), 589–593 (2021)